ARTICLE

Check for updates

Journal of
Sensor Science and Technology

The Korean Sensors Society

Enhanced Transmittance of Mid-Infrared Fabry–Pérot Filters via Annealed MgO Anti-Reflective Coatings on Silicon Substrates

Dong Geon Jung[1], Seongpil Hwang[1], and Daewoong Jung[2,3,+]

[1]*Mobility System R&D Group, Korea Institute of Industrial Technology (KITECH), Daegu 42994, Republic of Korea*
[2]*College of Nanoscience & Nanotechnology, Department of Nanomechatronics Engineering, Pusan National University, 2 Busandaehak-ro, Busan 46241, Republic of Korea*
[3]*University College, School of Transdisciplinary Engineering, Pusan National University, 2 Busandaehak-ro, Busan 46241, Republic of Korea*

Cite This: *J. Sens. Sci. Technol. Vol. 35, No. 3 (2026) 233-241*

https://doi.org/10.46670/JSST.2026.35.3.233

ABSTRACT: Mid-infrared (MIR) optical filters are critical components of non-dispersive infrared (NDIR) gas sensors. In this study, MgO anti-reflective (AR) coatings combined with thermal annealing were employed to enhance the transmittance of silicon-based Fabry–Pérot filters designed for CO_2 detection at 4.26 μm. An optimized MgO layer (~635 nm) increased the transmittance from 44.7% to 63.8%, while subsequent annealing further improved it to 70.1%. Microstructural analyses using XRD, SEM, and AFM revealed that annealing increased grain size and reduced grain boundary fraction (from 27.82% to 5.28%), leading to reduced optical scattering and reflection. This structural evolution was identified as the primary mechanism for transmittance enhancement. These results demonstrate that annealed MgO AR coatings provide an effective approach to improving the performance of MIR optical filters for NDIR CO_2 sensing applications.

KEYWORDS: *Infrared, Optical filter, Anti-reflective coating, Annealing*

1. INTRODUCTION

Infrared optical technologies have been widely utilized across diverse fields, including environmental monitoring, medical diagnostics, military, and space exploration [1-3]. Among gas sensors employed for environmental monitoring, various types have been developed, such as metal oxide semiconductor (MOS) sensors [4,5], non-dispersive infrared (NDIR) sensors [6,7], and electrochemical sensors [8,9]. In particular, non-dispersive infrared gas sensors have attracted significant attention in industrial applications for precise gas analysis due to their high accuracy, reliability, stability, and long operational lifetimes. One of the key components of these sensors is an infrared optical filter capable of selectively transmitting light within a highly specific wavelength range [10]. Enhancing the efficiency of such filters can significantly improve the accuracy and overall performance of the sensors.

This study aimed to enhance the transmittance of optical filters for non-dispersive infrared (NDIR) gas sensors. Optical filters commonly used in NDIR gas sensors are designed to operate within the mid-infrared (MIR) region, typically spanning wavelengths from 3 to 8 μm [11]. In this spectral range, various greenhouse gases—such as CH_4, CO_2, H_2O, and O_2—exhibit characteristic absorption features, and filters are therefore engineered with center wavelengths corresponding to the specific absorption bands of each gas. Among these gases, carbon dioxide is particularly representative, and there is a strong technological demand for optical filters operating at a wavelength of 4.26 μm for its detection in NDIR gas sensing applications [12].

Meanwhile, one effective approach to improving the transmittance of filter substrates is the application of anti-reflective (AR) coatings. AR coatings are a class of optical thin films widely employed to enhance the performance of optical devices. Typically applied to transparent surfaces such as lenses or glass, these coatings are designed to reduce unwanted reflection at over specific wavelength ranges while increasing overall transmittance.

Fabry–Pérot filters fabricated on silicon substrates, MgO-coated filters incorporating an anti-reflective (AR) layer, and MgO-coated filters subjected to additional annealing

[+]Corresponding author: dwjung@pusan.ac.kr
Received : May. 4, 2026, Revised : May. 14, 2026, Accepted : May. 18, 2026

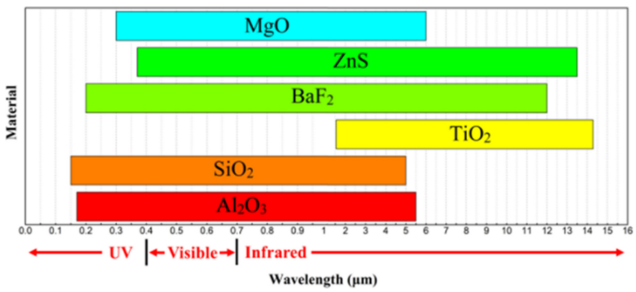

Fig. 1. Wavelength range by materials.

treatment were prepared, and their transmittance characteristics were comparatively analyzed. Through this controlled comparison, the effects of the MgO AR coating and its subsequent annealing on the performance of infrared filters were systematically investigated. Representative materials for optical thin-film coatings include Al_2O_3, SiO_2, TiO_2, BaF_2, ZnS, and MgO. The corresponding wavelength ranges of these materials are presented in Fig. 1 [13-16]. These materials effectively reduce reflectance at the surface of silicon substrates in the mid-infrared region, thereby enhancing optical transmittance.

Among these materials, magnesium oxide (MgO) exhibits excellent optical and physical properties. As a thin film, MgO has a refractive index of approximately 1.7 and a very low absorption coefficient of ~3.2×10^{-7}, enabling high transmittance over a broad spectral range from the ultraviolet to the infrared region [17,18]. Owing to these characteristics, MgO is considered a highly suitable material for optical filters in mid-infrared applications, including thermal imaging and spectroscopic analysis. Its low absorption contributes significantly to improving the efficiency of optical devices by minimizing optical losses.

In addition, MgO possesses a high melting point of approximately 2800°C, which provides excellent thermal stability and results in minimal thermal degradation during post-processing, even under high-temperature conditions.

In this study, MgO thin films were deposited and the annealing conditions were optimized to enhance optical transmittance, while the underlying mechanisms were elucidated through comprehensive material characterization. An optimized MgO anti-reflective (AR) coating was designed via simulation, and its implementation resulted in a transmittance improvement of up to 15.8% on a silicon substrate. Furthermore, the inherent decrease in transmittance with increasing layer number in distributed Bragg reflector (DBR) structures was effectively mitigated by applying the MgO AR coating, thereby demonstrating its capability to improve the optical performance of multilayer thin-film systems.

2. EXPERIMENTAL EQUIPMENTS

In this study, thin films were deposited using an electron-beam evaporation (E-beam) technique to achieve the desired film thickness. The transmittance of the fabricated filters was measured using a Fourier-transform infrared (FTIR) spectrometer (Nicolet 5700, Thermo Fisher Scientific). The surface morphology and microstructure of the coated films were analyzed by field-emission scanning electron microscopy (FE-SEM) (SU8600, Hitach) and atomic force microscopy (AFM) (AFM5300E, Hitach). In addition, the crystallinity of the annealed MgO coatings was investigated using X-ray diffraction (D8-DISCOVER, Bruker AXS).

The MgO thin films were deposited at room temperature under a vacuum level of 7.0×10^{-5} Torr using an electron-beam evaporator. During deposition, the film thickness was monitored in real time using a thickness monitoring system (STC-2002, Sycon). Post-deposition annealing of the films was carried out in ambient atmosphere using a furnace (FU-7MGE, Samhong Energy).

3. RESULTS AND DISCUSSIONS

3.1 Fabry–Pérot filters and DBR

The structure of a Fabry–Pérot filter consists of a central resonant cavity layer sandwiched between two highly reflective distributed Bragg reflectors (DBRs). Owing to this configuration, Fabry–Pérot filters exhibit high transmittance in the mid-infrared region. One of the most effective approaches to enhancing the selectivity and efficiency of filters based on Fabry–Pérot interferometry is the incorporation of distributed Bragg reflectors (DBRs). A DBR is composed of multiple alternating layers (N) with different refractive indices, enabling high reflectance at specific wavelength ranges.

The dependence of reflectance on the number of alternating layers in a DBR structure can be illustrated as shown in Fig. 2, where reflectance increases with increasing layer number. By integrating DBR structures with Fabry–Pérot interferometry, optical filters can be designed to selectively transmit target wavelengths even within the mid-infrared spectral region.

As shown in Table 1, Ge was selected as the high-refractive-index material and ZnS as the low-refractive-index material. Using these materials, a 13-layer Fabry–Pérot filter with optimized thicknesses was designed through simulation (VirtualLab Fusion, LightTrans.) and the results are presented in Fig. 3.

From the simulation results, the transmittance of the filters applied to quartz and silicon substrates was found to be 62.9% and 45.9%, respectively. Although the intrinsic transmittance

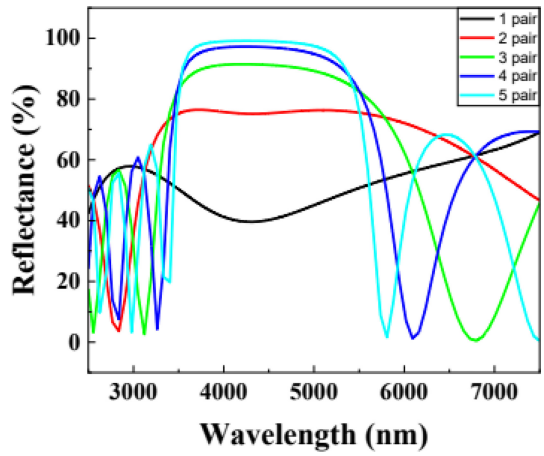

Fig. 2. Change in reflectance according to the number of Ge/ZnS pairs.

Table 1. Calculation of layer thickness using the refractive indices of ideal Ge and ZnS

Layer	Material	Refractive Index [n @λ = 4.26 μm]	Thickness (nm)
High index	Ge	4.0221	472.8
Low index	ZnS	2.2524	264.8
Cavity	ZnS	2.2524	945.6

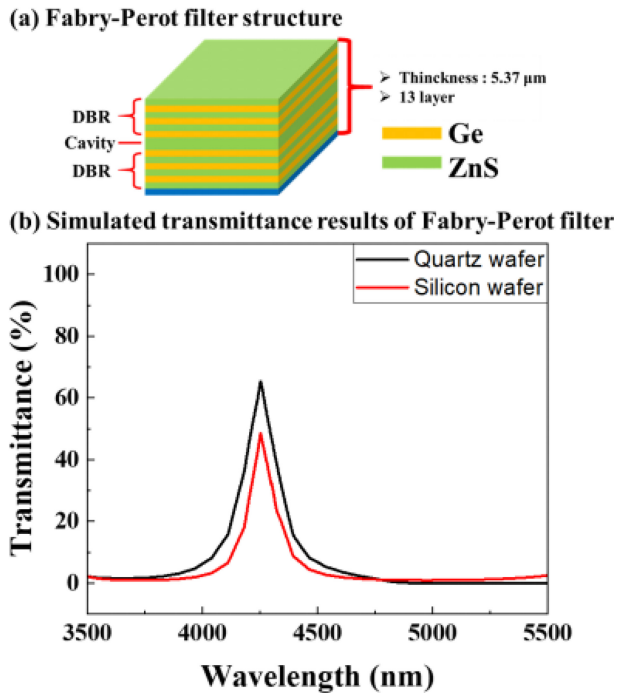

Fig. 3. (a) Designed Fabry–Pérot filter structure and (b) simulation results.

of the quartz and silicon substrates differed by approximately 20%, this difference decreased to about 17% after applying the filters. Nevertheless, due to the inherent transmittance difference between the substrates, the quartz-based filter still exhibited a higher transmittance than the silicon-based filter.

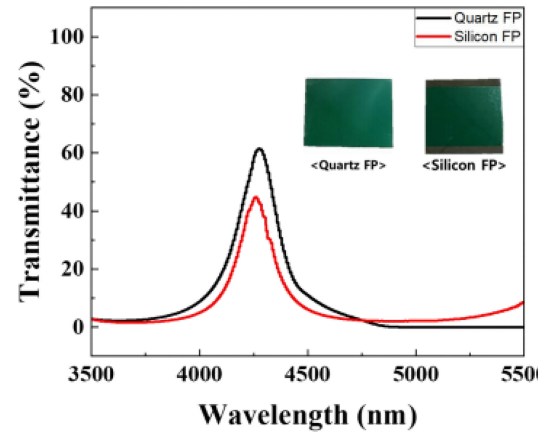

Fig. 4. Comparison of transmittance of Fabry–Pérot filter on fabricated quartz and silicon substrates.

In this study, for the detection of CO_2 using a non-dispersive infrared (NDIR) gas sensor, the optimal number of Ge/ZnS layer pairs in the distributed Bragg reflector (DBR) of the Fabry–Pérot filter was determined to be three pairs. The resulting filter structure consisted of a total of 13 layers with an overall thickness of 5.37 μm. Based on the simulation results, which indicated the highest transmittance for the Ge/ZnS combination, Fabry–Pérot filters were fabricated on both quartz and silicon substrates using these materials, and their transmittance was experimentally measured. As shown in Fig. 4, the measured transmittance of the fabricated filters on quartz and silicon substrates was 60.3% and 44.7%, respectively. Subsequently, the Fabry–Pérot filter with anti-reflective coating will be fabricated on silicon substrate, which is considerably less expensive than quartz substrate and offer superior compatibility with semiconductor processing, thereby facilitating fabrication.

3.2 Effect of anti-reflective (AR) coatings

As illustrated in Fig. 5, to achieve optimal transmittance at a specific wavelength, the thickness of the thin film should be one-quarter of the target wavelength. Under this condition, a half-wavelength optical path difference is generated between the incident light and the light reflected from the top and bottom interfaces of the thin film. Consequently, the two reflected waves exhibit a phase difference of exactly 180°, resulting in destructive interference that suppresses reflection.

Based on this principle, the optimal thickness of an AR coating can be determined using the refractive index (n) of the thin film and the target wavelength (λ) as follows.

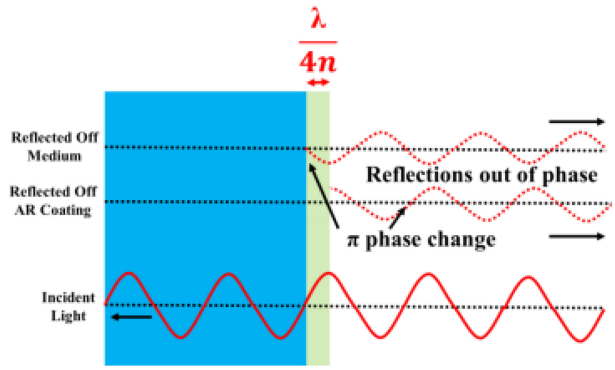

Fig. 5. Principle of increased light transmission with AR coating

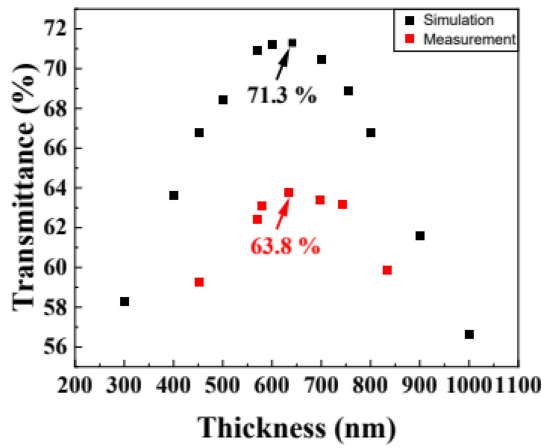

Fig. 6. Comparison of simulated transmittance results and actual measured values according to the thickness of MgO thin film

$$d = \lambda/4n \tag{1}$$

In this experiment, to detect CO_2 at its characteristic absorption wavelength of 4.26 μm, the designed thin-film thickness was set to λ/4n, corresponding to 641 nm, and a silicon substrate was employed.

To investigate the effect of MgO thin-film thickness on transmittance, MgO films with thicknesses of 452, 579, 635, 698, 742, and 833 nm were deposited using an electron-beam evaporation system. The transmittance of each sample was measured using FTIR spectroscopy, and the variation in transmittance at the 4.26 μm wavelength was analyzed as a function of film thickness.

As shown in Fig. 6, simulation results indicate that the transmittance increased from 44.7% to 71% (an improvement of approximately 16%) after the application of the anti-reflective coating. Although the fabricated filters exhibited a lower transmittance of approximately 63.8% compared to the simulated value, this still represents a significant improvement over the uncoated silicon substrate. The discrepancy between the simulated transmittance and measured transmittance is believed to arise from various fabrication process-related factors (e.g., thin film thickness deviations, film roughness, etc.). The optimal thickness was observed at 635 nm, while thinner or thicker films resulted in decreased transmittance. This observation is consistent with Eq. (1), which predicts an optimal thickness of 635 nm. The enhancement in transmittance after applying the AR coating is attributed to the following relationship.

Based on the law of conservation of energy, the energy of incident light (E_{inci}) can be expressed as the sum of the reflected energy (E_{ref}), transmitted energy (E_{trans}), and absorbed energy (E_{absor}), as given in Eq. (2):

$$E_{inci} = E_{ref} + E_{trans} + E_{absor} \tag{2}$$

Assuming that the amount of light absorbed in the thin film is negligible, Eq. (2) can be simplified according to the law of energy conservation as follows:

$$E_{inci} = E_{ref} + E_{trans} \tag{3}$$

By expressing Eq. (3) in terms of reflectance (R) and transmittance (T), the relationships can be written as Eqs. (4) and (5), respectively.

$$R + T = 1 \tag{4}$$

$$T = 1 - R \tag{5}$$

From the relationship between transmittance and reflectance, it can be observed that an increase in transmittance corresponds to a decrease in reflectance [18].

3.3 Effect of annealing treatment

It is well known that the optical properties of thin films are significantly influenced by post-treatment processes. To further enhance the transmittance of the optical filter, thermal annealing was performed. MgO thin films with an identical thickness of 635 nm, deposited under the same conditions, were annealed at different temperatures for 3 hours each. The annealing temperature ranged from 200°C to 1000°C in increments of 200°C. The upper limit of annealing temperature (1000°C) and heating rate (5°C/min) were selected due to wafer warping induced by the mismatch in thermal expansion coefficients between the silicon substrate and the MgO thin film.

Annealing was conducted in ambient atmosphere, with a heating rate of 5°C/min to reach the target temperature, followed by a 3-hour dwell time and subsequent natural cooling. As shown in Fig. 7, the transmittance of the MgO thin film varied with annealing temperature and time, with the highest transmittance observed at 1000°C for 3 hours, increasing from the initial 63.8% to 70.1%.

Table 2. Annealing treatment conditions of MgO thin film

Annealing treatment conditions		
Temperature	Time	Heating rate
200~1000°C	3 hours	5°C/min

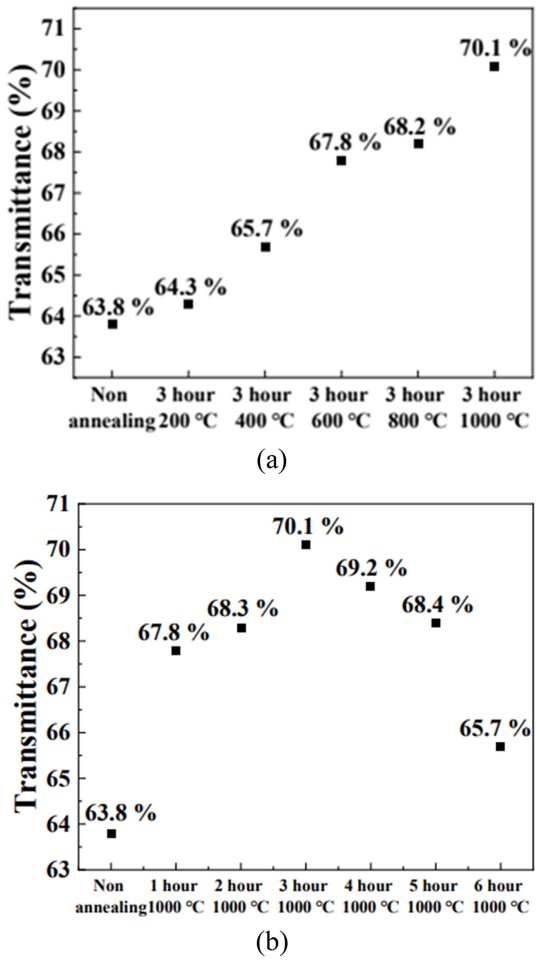

Fig. 7. Changes in transmittance after annealing according to (a) temperature and (b) time variations of MgO thin film.

As shown in Fig. 8, the XRD patterns of the annealed MgO thin films at different temperatures reveal that peaks corresponding to the (200) and (220) planes are present in all samples. However, an additional peak corresponding to the (111) plane appears in the films annealed at 800°C and 1000°C. The emergence of the (111) peak indicates that the MgO thin film exhibits characteristics of a face-centered cubic (FCC) structure [19].

The presence of the (111) and (200) diffraction peaks reflects the structural orientation and crystallinity of the MgO thin films, which can contribute to their effectiveness as optical filters, particularly in enhancing transmittance. Improved structural stability reduces internal light scattering, thereby increasing transmittance [20]. Furthermore, depending on the

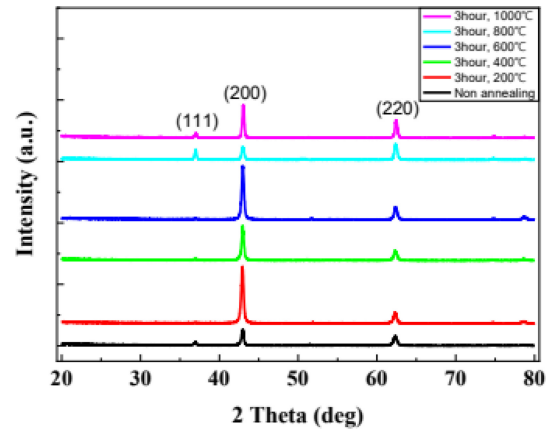

Fig. 8. The XRD results of MgO thin film according to annealing temperature changes.

surface roughness of the optical filter, incident light may undergo refraction, reflection, transmission, and scattering at the surface [21,22].

To minimize the loss of incident light arising from surface characteristics, the surface roughness was analyzed. In addition, the effect of annealing-induced changes in surface roughness on transmittance was investigated.

To examine the variation in transmittance as a function of surface roughness at optimized annealing temperatures, the annealing temperature was systematically controlled. The surface roughness of the MgO thin films after annealing was measured over an area of 1 μm^2 using atomic force microscopy (AFM). Fig. 9 presents the surface roughness results as a function of annealing temperature, with the annealing time fixed at 3 hours.

It was confirmed that the surface roughness (RMS, R_a) increases proportionally with increasing annealing temperature. As shown in Fig. 10, an increase in film temperature leads to an increase in surface roughness, which is accompanied by a corresponding increase in transmittance.

To elucidate the mechanism behind the transmittance enhancement as a function of annealing temperature and time, the grain size of the MgO thin films under each condition was analyzed using SEM. Fig. 11 presents the SEM results of grain size as a function of annealing temperature for a fixed annealing duration of 3 hours.

The average grain size of the as-deposited film (without annealing) was measured to be approximately 40 nm. As the annealing temperature increased to 200, 400, 600, 800, and 1000°C, the grain size correspondingly increased to 45, 42.8, 51.4, 69.5, and 108.9 nm, respectively.

Fig. 12 illustrates the transmittance trend of MgO thin films as a function of annealing temperature. As the annealing

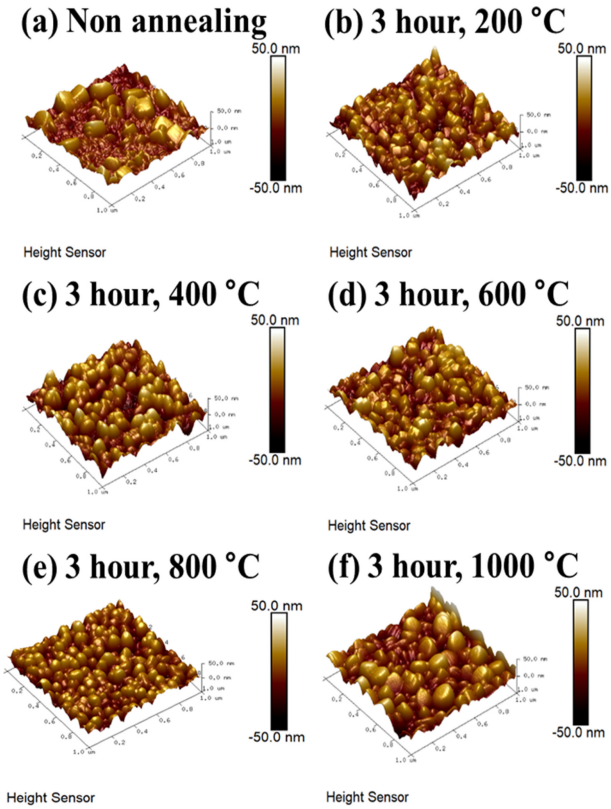

Fig. 9. The AFM results of MgO thin film according to annealing temperature changes (a) non annealing, (b) 200 °C, (c) 400 °C, (d) 600 °C, (e) 800 °C and (f) 1000 °C.

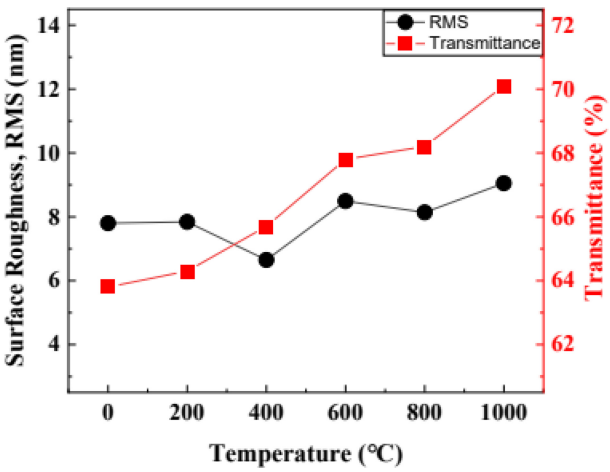

Fig. 10. Comparison of surface roughness and transmittance of MgO thin film according to annealing temperature changes.

temperature increased, both the grain size and the transmittance of the MgO films exhibit an increasing trend. The enhancement in transmittance with increasing annealing temperature is attributed to the reduction in the fraction of grain boundaries as the grain size increases, which leads to decreased reflection and refraction of incident light within the

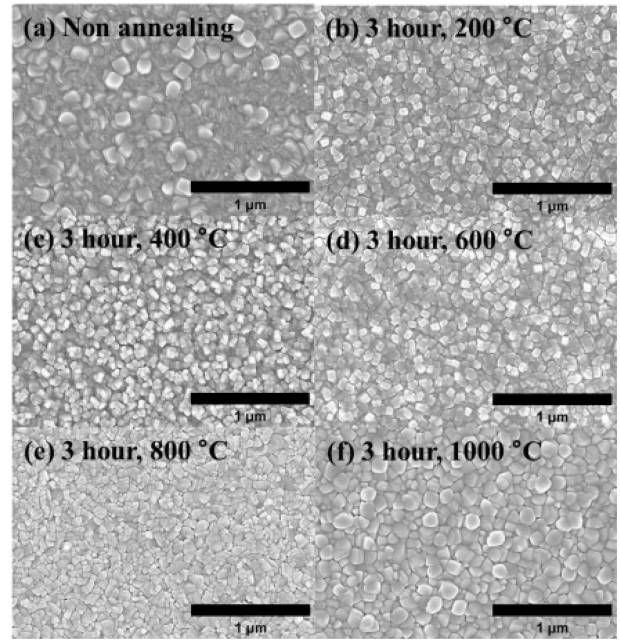

Fig. 11. The SEM results of MgO thin film according to annealing temperature changes (a) non annealing, (b) 200 °C, (c) 400 °C, (d) 600 °C, (e) 800 °C and (f) 1000 °C.

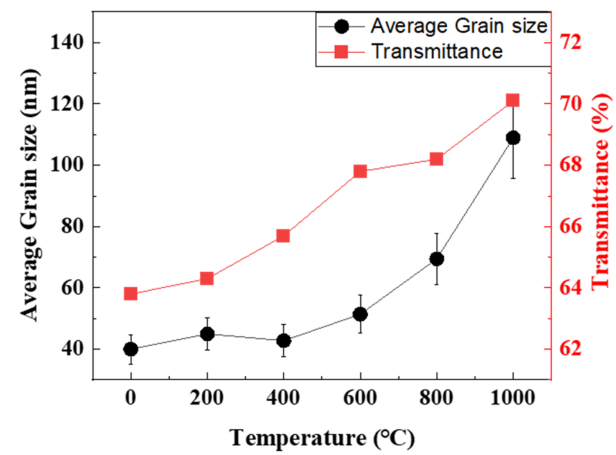

Fig. 12. Change in grain size and transmittance of MgO thin film according to annealing temperature.

thin film.

By correlating the SEM analysis of grain size with the FT-IR transmittance measurements, it can be concluded that both grain size and grain boundary density play significant roles in determining the optical transmittance of MgO thin films. Fig. 13 presents the analysis of grain boundary fraction as a function of annealing temperature, obtained by processing SEM images using ImageJ software.

In the absence of annealing, the grain boundary fraction was measured to be 27.82%. As the annealing temperature increased to 200, 400, 600, 800, and 1000°C, the grain

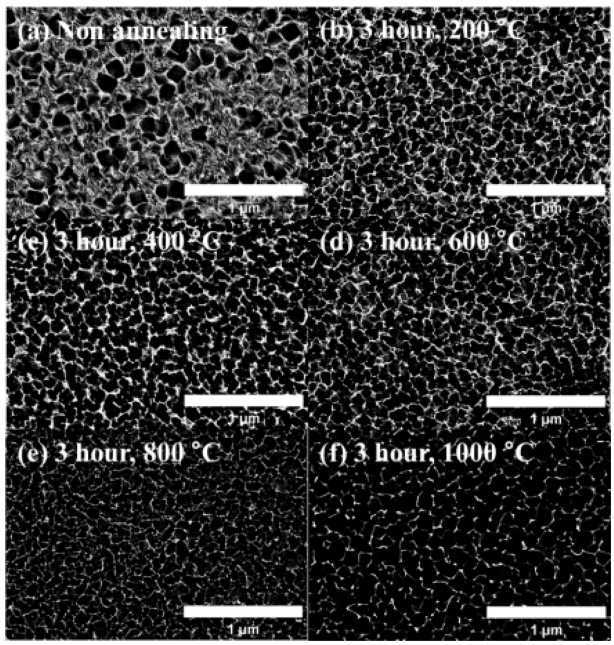

Fig. 13. Comparison of crystal structure of MgO thin film according to annealing temperature changes (a) non annealing, (b) 200°C, (c) 400°C, (d) 600°C, (e) 800°C and (f) 1000°C.

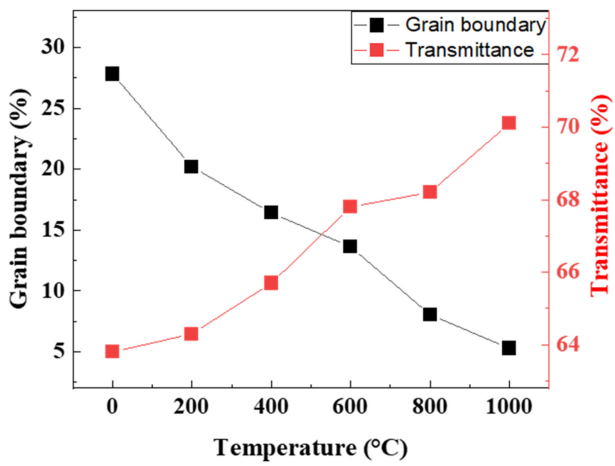

Fig. 14. Comparison of grain boundary ratios and transmittance of MgO thin film according to annealing temperature.

boundary fraction decreased to 20.2%, 16.4%, 13.62%, 8.05%, and 5.28%, respectively. Fig. 14 presents the relationship between the grain boundary fraction and the transmittance of MgO thin films as a function of annealing temperature. It can be clearly observed that the transmittance increases as the grain boundary fraction decreases.

The relationship between grain size and grain boundary fraction was examined in relation to the transmittance enhancement of MgO thin films induced by annealing. Incident light is significantly influenced by both the grain size and the grain boundaries within the film, as shown in Fig. 15.

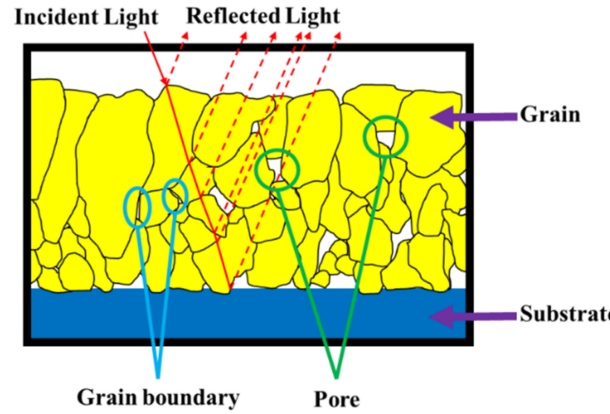

Fig. 15. Optical path of incident and reflected light in AR coating according to grain size and grain boundary fraction

When the grain size is larger and the grain boundary fraction is lower, the amount of reflected light decreases, resulting in an increased proportion of light transmitted through the thin film.

With increasing annealing temperature, the grain size of the MgO thin films increased, and by extending the annealing time, conditions were achieved that yielded the largest grain size and the lowest grain boundary fraction.

Therefore, this study confirms that the improvement in transmittance of MgO thin films through annealing is primarily attributed to the increase in grain size and the reduction in grain boundary fraction, which together reduce light reflection and enhance light transmission [23,24].

4. CONCLUSIONS

In this study, MgO anti-reflective (AR) coatings deposited by electron-beam evaporation were annealed to fabricate infrared optical filters operating at a wavelength of 4.26 μm, and the resulting enhancement in transmittance was analyzed through detailed investigation of the thin-film microstructure. By varying the annealing temperature, the grain size of the MgO coatings was significantly increased while the grain boundary fraction was reduced, leading to improved optical transmittance.

By applying the MgO AR coating annealed under optimized conditions to a silicon substrate with an initial transmittance of approximately 44.7%, a maximum transmittance of 70.1% was achieved, demonstrating its effectiveness in enhancing the performance of silicon-based Fabry–Pérot filters. In addition, this study optimized the annealing conditions for single-layer MgO thin films and established the relationship between transmittance and the evolution of grain size and grain boundary fraction in the deposited films.

These findings are expected to provide a viable approach

to overcoming transmittance limitations in both broadband and narrowband optical filters. Furthermore, the proposed strategy can be applied to mid-infrared non-dispersive infrared (NDIR) CO_2 sensors as well as other greenhouse gas sensing systems, potentially improving both sensitivity and selectivity.

CRediT Authorship Contribution Statement

Dong Geon Jung: Conceptualization, Methodology, Investigation, Data curation, Visualization, Writing – original draft. **Seongpil Hwang:** Formal analysis, Validation, Visualization, Writing – review and editing. **Daewoong Jung:** Supervision, Project administration, Funding acquisition, Validation, Writing – review and editing.

Declaration of Competing Interest

The authors declare that they have no competing financial interests or personal relationships that may have influenced the work reported in this study.

Acknowledgements

This study is a 2024 SME Technology Innovation Development Export-Oriented (Tech-Bridge) R&D project of the Small and Medium Business Technology Information Promotion Agency (SME Technology Innovation Development Institute), and is a study on Development of 8-Channel Total Organic Carbon (TOC) Measuring Device for Regular Monitoring of Water Quality of Waste Water and Process Water (RS-2024-00469087).

This work was supported by KOITA grant funded by MSIT(1711199734).

This study has been conducted with the support of the Korea Institute of Industrial Technology as “Development of Core Materials and Components for Quantum Sensing (Kitech UR-26-0064)”.

REFERENCES

[1] B. Mizaikoff, Infrared optical sensors for water quality monitoring, Water Sci. Technol. 47 (2003) 35–42.

[2] H. Guo, Z. Li, Application of medical infrared thermal imaging in the diagnosis of human internal focus, Infrared Phys. Technol. 101 (2019) 127–132.

[3] A. Sijan, Development of military lasers for optical countermeasures in the mid-IR, Proceedings of the Technologies for Optical Countermeasures VI, Berlin, Germany, 2009, p. 748304.

[4] D. Tyagi, H. Wang, W. Huang, L. Hu, Y. Tang, Z. Guo, et al., Recent advances in two-dimensional-material-based sensing technology toward health and environmental monitoring applications, Nanoscale 12 (2020) 3535–3559.

[5] T.V.K. Karthik, L. Martinez, V. Agarwal, Porous silicon ZnO/SnO_2 structures for CO_2 detection, J. Alloys Compd. 731 (2018) 853–863.

[6] H. Liu, Y. Shi, T. Wang, Design of a six-gas NDIR gas sensor using an integrated optical gas chamber, Opt. Express 28 (2020) 11451–11462.

[7] S. Esfahani, A. Tiele, S.O. Agbroko, J.A. Covington, Development of a tuneable NDIR optical electronic nose, Sensors 20 (2020) 6875.

[8] M. Struzik, I. Garbayo, R. Pfenniger, J.L.M. Rupp, A simple and fast electrochemical CO_2 sensor based on $Li_7La_3Zr_2O_{12}$ for environmental monitoring, Adv. Mater. 30 (2018) 1804098.

[9] H. Wang, H. Chen, M. Zhang, J. Wang, J. Sun, Solid-state potentiometric CO_2 sensor combining Li_3PO_4 with MoO_3-doped Li_2CO_3 sensing electrode, Ionics 25 (2019) 3397–3406.

[10] A. Schmidt-Bleker, J. Winter, S. Iseni, M. Dünnbier, K.-D. Weltmann, S. Reuter, Reactive species output of a plasma jet with a shielding gas device—combination of FTIR absorption spectroscopy and gas phase modelling, J. Phys. D Appl. Phys. 47 (2014) 145201.

[11] B.M. Walsh, H.R. Lee, N.P. Barnes, Mid infrared lasers for remote sensing applications, J. Lumin. 169 (2016) 400–405.

[12] G. Zhang, X. Wu, A novel CO2 gas analyzer based on IR absorption, Opt. Lasers Eng. 42 (2004) 219–231.

[13] A.P. Chernyshev, V.A. Petrov, V.E. Titov, A.Yu. Vorobyev, Thermal radiative properties of magnesium oxide at high temperatures, Thermochim. Acta 218 (1993) 195–209.

[14] M. Debenham, Refractive indices of zinc sulfide in the 0.405–13-μm wavelength range, Appl. Opt. 23 (1984) 2238–2239.

[15] I.H. Malitson, Refractive properties of barium fluoride, J. Opt. Soc. Am. 54 (1964) 628–632.

[16] J. Kischkat, S. Peters, B. Gruska, M. Semtsiv, M. Chashnikova, M. Klinkmüller, et al., Mid-infrared optical properties of thin films of aluminum oxide, titanium dioxide, silicon dioxide, aluminum nitride, and silicon nitride, Appl. Opt. 51 (2012) 6789–6798.

[17] D.M. Roessler, D.R. Huffman, Magnesium Oxide (MgO), In: E. D. Palik (Ed.), Handbook of Optical Constants of Solids, Academic Press, San Diego, 1997, pp. 919–955.

[18] R. Hanna, Infrared properties of magnesium oxide, J. Am. Ceram. Soc. 48 (1965) 376–380.

[19] B.A. Taleatu, E. Omotoso, C. Lal, W.O. Makinde, K.T. Ogundele, E. Ajenifuja, et al., XPS and some surface characterizations of electrodeposited MgO nanostructure, Surf. Interface Anal. 46 (2014) 372–377.

[20] S. Valanarasu, V. Dhanasekaran, M. Karunakaran, T.A. Vijayan, R. Chandramohan, T. Mahalingam, Microstructural, optical and electrical properties of various time annealed spin coated MgO thin films, J. Mater. Sci. Mater. Electron. 25 (2014) 3846–3853.

[21] A.A. Maradudin (Ed.), Light Scattering and Nanoscale Surface Roughness, Springer Science & Business Media, New York, 2010.

[22] N.O. Myers, Characterization of surface roughness, Wear 5 (1962) 182–189.

[23] N. Juntavee, S. Attashu, Effect of sintering process on color parameters of nano-sized yttria partially stabilized tetragonal monolithic zirconia, J. Clin. Exp. Dent. 10 (2018) e794–e804.

[24] H.J. Ma, W.K. Jung, C. Baek, D.K. Kim, Influence of microstructure control on optical and mechanical properties of infrared transparent Y_2O_3-MgO nanocomposite, J. Eur. Ceram. Soc. 37 (2017) 4902–4911.